Inorg. Chem. **2003**, *42*, 4898–4901

Synthesis, Structure, and Properties of the New Intermetallic Compounds $SrPdTl_2$ and $SrPtTl_2$

Shengfeng Liu and John D. Corbett*

Ames Laboratory[1] *and Department of Chemistry, Iowa State University, Ames, Iowa 50010*

Received March 7, 2003

The title compounds have been synthesized and characterized structurally and through property measurements and electronic structure calculations. Single-crystal X-ray diffraction analyses reveal that the two compounds crystallize in an orthorhombic system, $MgCuAl_2$ type (*Cmcm*, $Z = 4$, $a = 4.486(2)$, 4.491(3) Å, $b = 10.991(5)$, 10.990(6) Å, $c = 8.154(1)$, 8.140(4) Å for $SrPdTl_2$, and $SrPtTl_2$, respectively). The structure can be directly derived from that of hexagonal $SrTl_2$ ($CaIn_2$ type) in which four-bonded thallium atoms in shared puckered hexagons generate tunnels. The Pd or Pt is encapsulated (with symmetry reduction) on the side of each tunnel within a distorted trigonal prism. Band structure calculations (EHTB) on both $SrTl_2$ and $SrPdTl_2$ demonstrate the effects of the conversion, with strong Pd–Tl bonding and appreciable electron transfer from Tl to Pd. Property measurements show that $SrPdTl_2$ is metallic, as expected.

Introduction

In recent years, a large number of new binary and ternary trielide (Ga−Tl) and tetrelide (Si−Pb) compounds with the active metals have been found with unusual cluster or framework anions and diverse electrical and magnetic properties.[2,3] Among binary alkali-metal−indium compounds, a variety of different and sometimes large indium examples exist, such as hypoelectronic In_{11}^{7-} ions and *closo*-In_{16} and *nido*-In_{11} clusters in networks.[4−6] More recent explorations of the lesser-known alkaline-earth-metal−trielide systems have led to discoveries of hypoelectronic phases, $SrIn_4$[7] and Sr_3In_5,[8] for example. Compared with indium, the corresponding thallium systems appear somewhat richer in compounds that contain individual thallium cluster anions. These include not only classical clusters but also hypoelectronic examples, e.g., Tl_7^{7-} in $K_{10}Tl_7$,[9] Tl_9^{9-} in $Na_2K_{21}Tl_{19}$,[10] and Tl_{11}^{7-} in K_8Tl_{10}.[11]

The substitution in, or addition of transition metals to, some of the alkali-metal−triel systems results not only in new ternary compounds but also in the appearance of a family of novel centered clusters. Substitution of one indium atom by mercury in K_8In_{11}, which is characteristically metallic and Pauli paramagnetic, yields the isotypic but diamagnetic semiconductor $K_8In_{10}Hg$,[12] whereas new centered clusters exist in $K_8In_{10}Zn$,[13] $K_8Tl_{10}Zn$,[14] and $Na_{10}Ga_{10}Ni$.[15] Some explorations of ternary indium-rich compounds containing both alkaline-earth and transition (d) metals have also resulted in the discovery of the ternary compounds $CaNiIn_4$, Ca_2CuIn_3,[16] and $CaTIn_2$ (T = Pd, Pt, Au).[17]

In contrast to the foregoing indium−transition metal systems, no such chemistry of the corresponding thallium systems has been reported. Our recently initiated explorations

* Author to whom correspondence should be addressed. E-mail: jdc@ameslab.gov.

(1) This research was supported by the Office of the Basic Energy Sciences, Materials Sciences Division, U.S. Department of Energy (DOE). The Ames Laboratory is operated for DOE by Iowa State University under Contract No. W-7405-Eng-82.

(2) Corbett, J. D. In *Chemistry, Structure and Bonding of Zintl Phases and Ions*; Kauzlarich, S. M., Ed.; VCH Publishers: New York, 1996; Chapter 4.
(3) Corbett, J. D. *Angew. Chem., Int. Ed.* **2000**, *39*, 670.
(4) Sevov, S. C.; Corbett, J. D. *Inorg. Chem.* **1991**, *30*, 4875.
(5) Sevov, S. C.; Corbett, J. D. *Inorg. Chem.* **1992**, *31*, 1895.
(6) Sevov, S. C.; Corbett, J. D. *J. Solid State Chem.* **1993**, *103*, 114.
(7) Seo, D.-K.; Corbett, J. D. *J. Am. Chem. Soc.* **2000**, *122*, 9621.
(8) Seo, D.-K.; Corbett, J. D. *J. Am. Chem. Soc.* **2001**, *123*, 4512.
(9) Kaskel, S.; Corbett, J. D. *Inorg. Chem.* **2000**, *39*, 3086.
(10) Dong, Z.-C.; Corbett, J. D. *J. Am. Chem. Soc.* **1994**, *116*, 3429.
(11) Dong, Z.-C.; Corbett, J. D. *J. Cluster Sci.* **1995**, *6*, 187.
(12) Sevov, S. C.; Corbett, J. D. Ostenson, *J. Alloys Compd.* **1993**, *202*, 289.
(13) Sevov, S. C.; Corbett, J. D. *Inorg. Chem.* **1993**, *32*, 1059.
(14) Dong, Z.-C.; Corbett, J. D. *Inorg. Chem.* **1997**, *36*, 3559.
(15) Henning, R. W.; Corbett, J. D. *Inorg. Chem.* **1999**, *38*, 3883.
(16) Sysa, L. V.; Kalychak, Ya. M. *Crystallogr. Rep.* **1993**, *38*, 278.
(17) Hoffmann, R.-D.; Pöttgen, R.; Landrum, G. A.; Dronskowski, R.; Künen, B.; Kotzyba, G. *Z. Anorg. Allg. Chem.* **1999**, *625*, 789.

10.1021/ic030089k CCC: $25.00
Published on Web 07/08/2003

Table 1. Lattice Parameters (Å, Å^3) of Orthorhombic (*Cmcm*) $SrPdTl_2$ and $SrPtTl_2$[a]

compound	*a*	*b*	*c*	*V*
$SrPdTl_2$	4.486(2)	10.991(5)	8.154(1)	402.0 (3)
$SrPtTl_2$	4.491(3)	10.990(6)	8.140(4)	401.8 (4)

[a] Refined from Guinier powder data with Si as internal standard, λ = 1.540562 Å, 23 °C.

of these have led to two new phases, $SrPdTl_2$ and $SrPtTl_2$, for which we here report their syntheses, structures, bonding characteristics, and physical properties.

Experimental Section

Synthesis. All reactions were carried out within welded Nb tubes jacketed in a fused silica container, as described previously.[5] The elements used, Sr (99.9%), Pd (99.95%), and Tl (99.999%), were all from Alfa-Aesar. All materials were handled in N_2- or He-filled gloveboxes with moisture levels below 0.1 ppm by volume. The surfaces of thallium were cut clean with a scalpel just before use.

No ternary phase diagrams are available for these ternary systems. Following both the binary Sr−Tl phase diagram[18] and our experiences, reaction mixtures were usually first heated at 1050 °C and then annealed at 600 °C. Single crystals were first found with the loaded composition $SrPdTl_{2.2}$ that had been so reacted, quenched to preserve a finely divided mixture of the components, annealed for 7 days, and then cooled to room temperature at 5 °C/h. Subsequently, high-purity (>95%) single phases of $SrPdTl_2$ and $SrPtTl_2$ were obtained after stoichiometric syntheses from the constituent elements that were similarly reacted but annealed for 2 weeks. The purity judgment came from comparisons of their Guinier powder patterns with those calculated for the refined structure. The structure was not formed when Pt or Pd was substituted by Zn, Rh, Ir, or Au.

X-ray powder patterns from samples mounted between pieces of cellophane were collected with the aid of an Enraf-Nonius Guinier camera, Cu Kα radiation (λ = 1.540 562 Å), and NIST silicon as an internal standard. Least-squares refinements of 20 and 21 lines for $SrPdTl_2$ and $SrPtTl_2$, respectively, that had been indexed on the basis of the refined structural model resulted in the lattice constants given in Table 1.

Structure Determination. A silvery block-shaped crystal of $SrPdTl_2$, 0.2 × 0.25 × 0.15 mm, was mounted in a glass capillary inside the glovebox. The crystal was first checked by Laue photography and then transferred to a Bruker APEX SMART CCD-equipped X-ray diffractometer for data collection, which took place at 23 °C with monochromated Mo Kα radiation. A total of 1315 frames were collected with the exposure time of 10 s/frame. The reflection intensities were integrated with the SAINT subprogram in the SMART software package,[19] and SADABS was applied for the absorption correction (μ = 96.97 mm^{-1}). The XPREP subprogram in the SHELXTL software package[20] was used for the space group determination, in which systematic absences indicated *Cmcm*, *Cmc*2_1, and *C*2*cm* as possible space groups. The intensity statistics showed a clear indication of a centrosymmetry ($\langle E^2 - 1 \rangle$ = 0.985), and the centric space group *Cmcm* gave satisfactory refinement results. Application of direct methods via SHELXTL revealed all of the atom positions. The full-matrix least-squares refinement converged at $R(F)$ = 3.75%, wR2 = 10.18%, for data with $I/\sigma(I)$ > 2. The largest positive and negative residuals in the ΔF map were 2.96 and −4.00 e$^-$ Å^{-3}, respectively. Some data collection and refinement parameters are listed in Table 2. Table 3 gives the atomic positional and equivalent isotropic displacement parameters, and Table 4 lists important interatomic distances. More detailed crystallographic information and the anisotropic displacement parameters are available in the Supporting Information.

Table 2. Crystal Refinement Data for $SrPdTl_2$

fw	602.76
space group, Z[a]	*Cmcm* (No. 63), 4
d_{calcd} (Mg/m^3)	9.928
μ (Mo Kα) (cm^{-1})	969.7
final R indices[b]	
R1, wR2 [$I > 2\sigma(I)$]	0.038, 0.102
R1, wR2 (all data)	0.042, 0.106

[a] Cell dimensions in Table 1. [b] $R1 = \sum||F_o| - |F_c||/\sum|F_o|$; $wR2 = \sum w(|F_o|^2 - |F_c|^2)^2/\sum w(F_o^2)]^{1/2}$.

Table 3. Atomic Coordinates (×10^4) and Isotropic-Equivalent Displacement Parameters (Å^2 × 10^3) for $SrPdTl_2$

	positions	*x*	*y*	*z*	*U*(eq)[a]
Tl	8f *m*..	0	1468(1)	5516(1)	11(1)
Pd	4c *m*2*m*	0	2817(2)	2500	11(1)
Sr	4c *m*2*m*	0	5652(2)	2500	11(1)

[a] *U*(eq) is defined as one-third of the trace of the orthogonalized $\mathbf{U}_{ij}$ tensor.

Table 4. Important Atom Separations (Å) in $SrPdTl_2$

Tl−Pd	2.871(2)	Pd−Tl × 2	2.871(2)
Tl−Pd × 2	2.879(2)	Pd−Tl × 4	2.879(2)
Tl−Tl	3.234(2)	Pd−Sr	3.120(3)
Tl−Tl × 2	3.306(2)	Pd−Sr × 2	3.276(2)
Tl−Tl	3.338(2)	Sr−Pd	3.120(3)
Tl−Sr × 2	3.450(2)	Sr−Pd × 2	3.276(2)
Tl−Sr	3.560(3)	Sr−Tl × 4	3.450(2)
Tl−Sr × 2	3.621(2)	Sr−Tl	3.560(3)
		Sr−Tl × 3	3.621(2)

Properties. Electrical resistivities of $SrPdTl_2$ and $SrTl_2$ were measured at 34 MHz over 110−251 K by the electrodeless "Q" method with the aid of a Hewlett-Packard 4342A Q meter.[21] The method is particularly suitable for measurements on air-sensitive samples for which large single crystals are not available. For this purpose, 54.2 mg or 86.7 mg of a powdered sample with grain diameters between 150 and 250 μm was dispersed with chromatographic alumina and sealed under He in a Pyrex tube. Magnetic susceptibility measurements were carried out at 3 T over 8−350 K on a Quantum Design (MPMS) SQUID magnetometer. The 102.6 mg of a $SrPdTl_2$ powdered sample was held between the faces of two fused silica rods that were in turn fixed and sealed inside a longer silica tube. M vs H data were checked at 5 K to ensure the absence of significant magnetic impurities.

EHTB Calculations. Extended Hückel tight-binding (EHTB) band calculations were carried out using the CAESAR program developed by Whangbo and co-workers.[22] The H_{ii} (eV) and ζ parameters utilized for EHTB band calculations were as follows. Sr: 5s −6.62, 1.214; 5p −3.92, 1.214.[23] Tl: 6s −11.6, 2.52; 6p −5.8, 1.77 (the most contracted set[24]). Pd: 5s −7.32, 2.19; 5p −3.75, 2.152; 4d: −12.02, ς_1 = 5.983, C_1 = 0.5535, ς_2 = 2.613, C_2 = 0.6701.[25]

(18) Bruzzone, G.; Francschi, E.; Merlo, F. *J. Less-Common Met.* **1978**, *60*, 59.
(19) *SMART*; Bruker AXS, Inc.; Madison, WI, 1996.
(20) *SHELXTL*; Bruker AXS, Inc.; Madison, WI, 1997.
(21) Zhao, J. T.; Corbett, J. D. *Inorg. Chem.* **1995**, *34*, 378.
(22) Ren, J.; Liang, W.; Whangbo, M.-H. *CAESAR for Windows*; Prime-Color Software, Inc.: North Carolina State University: Raleigh, NC, 1998.
(23) Hinze, J.; Jaffe, H. H. *J. Chem. Phys*. **1963**, *67*, 1501.

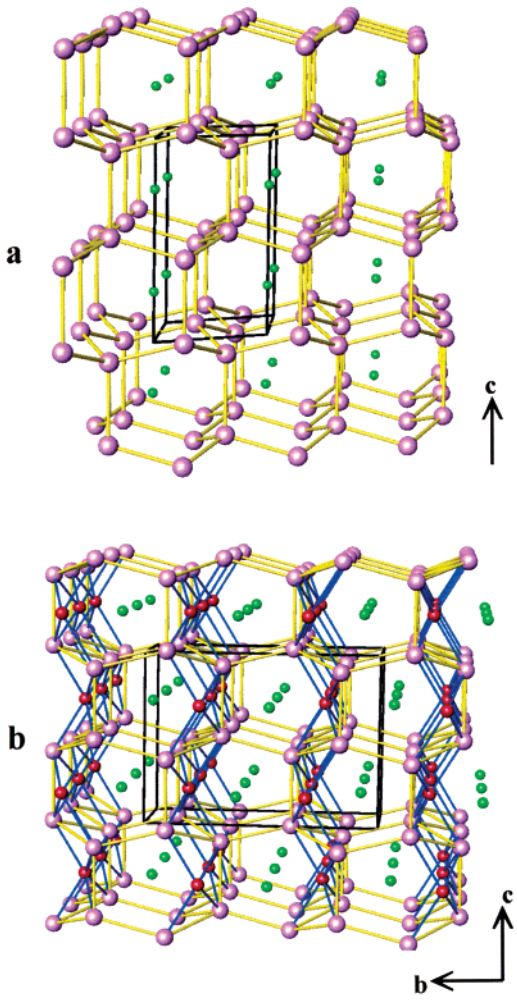

Figure 1. (a) ~[130] view of the parent structure $SrTl_2$ ($P6_3/mmc$).[27] The lavender spheres mark the Tl positions; green, Sr. Notice the tunnels built of fused puckered 6-rings of Tl (yellow interconnections) or, alternatively, the zigzag chains of Tl along $\vec{a}$ that are interconnected in the *bc* plane. (b) The equivalent ~[100] projection of the orthorhombic (*Cmcm*) structure of $SrPdTl_2$ with the encapsulated Pd (red) and very similar tunnels built by Tl−Tl (yellow) interconnections.

Results and Discussion

Structure. The new ternary compounds $SrPdTl_2$ and $SrPtTl_2$ are isostructural with the parent $MgCuAl_2$[26] and the more closely related $CaTIn_2$, T = Pd, Pt, Au.[17] The structure devolves in a regular way from the hexagonal structure ($P6_3/mmc$) of $SrTl_2$[27] ($CaIn_2$ type), which is illustrated in Figure 1a in a view along the *a* axis and with the *c* axis vertical. The 3D connection of 4-bonded thallium(−1) (4b-Tl^-) in puckered 6-rings forming a single type of tunnel along $\vec{a}$ is one of the simpler ways of achieving a Zintl phase structurally with 4b-Tl^-, although it appears that the phase is actually not closed shell electronically. Bonding of Pd etc. in distorted trigonal prismatic sites occurs at one side of each tunnel with a descent in symmetry to the orthorhombic subgroup *Cmcm*, as illustrated in Figure 1b with the *c* axis again vertical. The Pd atoms are located in rows on alternate sides of the tunnels along the *c* direction. A slightly different look at the structures in Figure 1 leads to the recognition of a network of zigzag chains of Tl that run along *a* and are interconnected by perpendicular bond formation parallel to the *b*−*c* planes. In fact, zigzag chains exist in a variety of solid-state frameworks, including $SrIn_4$[6] and Sr_3In_5[7] recently studied by us in which double zigzag chains are joined directly to generate much narrower channels.

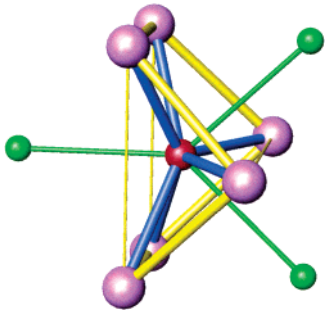

Figure 2. The environment of palladium in $SrPdTl_2$. The Sr, Pd, and Tl atoms are green, red, and lavender, respectively. The trigonal prismatic Tl about Pd is marked in yellow.

Distances in the $SrPdTl_2$ structure are quite regular. Those for Tl−Tl vary only over a small range, 3.234(2)−3.338(2) Å, and the palladium likewise has six Tl neighbors, all at 2.875 Å within a very small spread. As depicted in Figure 2, the $PdTl_6$ figure (after rotation by 90°) consists of a distorted trigonal prism of Tl about Pd that is tricapped on the rectangular faces by Sr. Retention of the basic tunnel structure means that the Tl−Tl prismatic edge toward the center of the cage is 1.20 Å longer. The change from $SrTl_2$ to $SrPdTl_2$ results in an increase in *d*(Tl−Tl) within the zigzag chains from 3.03 to 3.31−3.34 Å, and a contraction in the distance between zigzag chain from 3.32 to 3.23 Å, the Pd bonding thus producing somewhat more uniform distances within the thallium network.

Chemical Bonding and Electronic Structure. Electronic band structures were calculated for both $SrPdTl_2$ and $SrTl_2$ within the extended Hückel tight-binding (EHTB) approximation. The resulting total and projected partial densities-of-states (DOS) and the crystal orbital overlap populations (COOP) are plotted in Figures 3 and 4, respectively. The 72 valence electrons per cell in $SrPdTl_2$ fill the bands to a Fermi energy of −6.39 eV, and this cuts through a valence band composed mainly of thallium states, indicating that the compound should be metallic. This result is in accord with our experiences with the overarching covalency in such cluster phases as Sr_3In_5,[28] and the absence of closed-shell Pb^{-4}, Bi^{-3} states in some fairly simple compounds.[29,30] The natural expectation is that analogous Tl^{-5} states/closed shells are even less likely, particularly with these higher charged cations and the strongly interacting Pd. The Tl contributions are, in fact, spread over a wide range of energy. Narrow

(24) (a) Whitmire, K. H.; Ryan, R. R.; Wasserman, H. J.; Albright, T. A.; Kang, S. K. *J. Am. Chem. Soc.* **1986**, *108*, 6831. (b) Janiak, C.; Hoffmann, R. *J. Am. Chem. Soc.* **1990**, *112*, 5924.
(25) Alvarez, S. Table of Parameters for Extended Hückel Calculations, Part 1, Barcelona, Spain, 1987.
(26) Perlitz, H.; Westgren, A. *Ark. Kemi, Mineral. Geol.* **1943**, *16B*, 1.
(27) Iandelli, A. *Z. Anorg. Allg. Chem.* **1964**, *330*, 221.
(28) Klem, M. T.; Vaughey, J. T.; Harp, J. G.; Corbett, J. D. *Inorg. Chem.* **2001**, *40*, 7020.
(29) Li, B.; Mudring, A.-V.; Corbett, J. D. *Inorg. Chem.*, accepted.
(30) Guloy, A.; Mudring, A.-V.; Corbett, J. D. *Inorg. Chem.*, submitted.

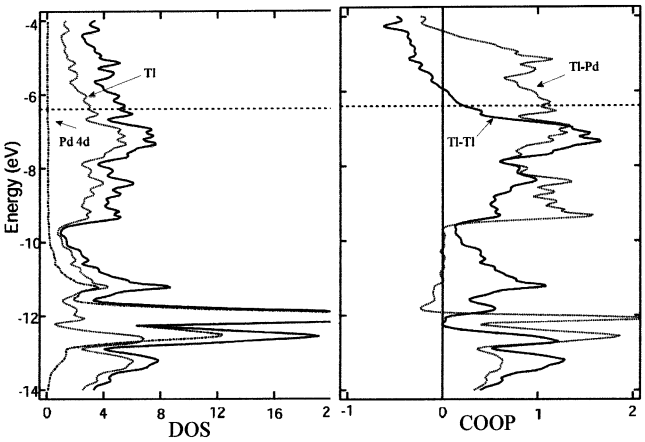

Figure 3. Densities-of-states (DOS) and the crystal orbital overlap population (COOP) results for $SrPdTl_2$. Left: the solid, dotted, and dash−dot curves represent total DOS and the partial DOS of Tl and Pd 4d, respectively. Right: The solid and dotted COOP values for all Tl−Tl and Tl−Pd contacts, respectively.

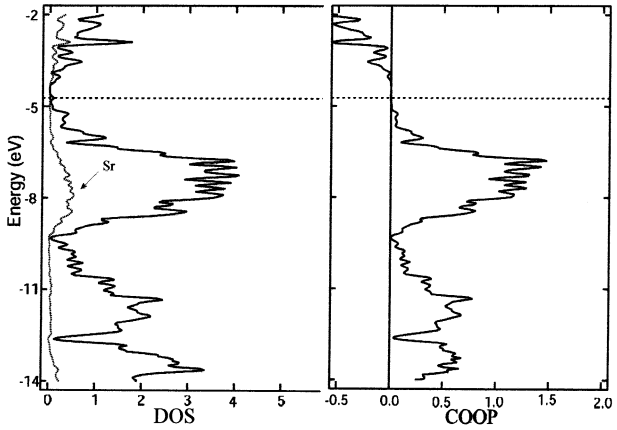

Figure 4. Comparative DOS and COOP data for $SrTl_2$. Left: The solid and dotted lines refer to total DOS and the partial DOS of Sr, respectively. Right: COOP data for Tl−Tl contacts.

low-lying Pd d-bands are localized around −12 eV, well below E_F. The contributions of strontium below the Fermi level are small at this approximation, although appreciable effects from the 4d levels thereon are to be expected. The suggestion in the COOP curves for $SrPdTl_2$ that there are insufficient electrons to utilize all Tl−Tl bonding states does not lead to the alternate incorporation of Au instead, although this alone is a generally insufficient basis for a good prediction.

The effect of insertion of transition metals into the structure of $SrTl_2$ can also be seen by comparing the calculated results for the electronic structure of binary $SrTl_2$, Figure 4, with those for $SrPdTl_2$, Figure 3. (Note that the $SrTl_2$ calculations were based on the positional parameters determined from powder data.[27]) A very low DOS or perhaps a gap of approximately 1.1 eV is indicated above a −4.73 eV Fermi level for $SrTl_2$, the latter comparing with a lower Fermi level of −6.39 eV and a broader band after insertion of Pd in $SrPdTl_2$. Based on experience,[28−30] we do not have great confidence that the EHTB method is sufficient for such a prediction, and our own measurements give $\rho_{300} \sim 18\ \mu\Omega$ cm for $SrTl_2$ with a metal-like temperature dependence. The general effect of Pd addition to $SrTl_2$ is to broaden the Tl−Tl contributions and to introduce substantial Tl−Pd bonding over a wide range of energy. The *approximate* charges according to EHTB are Tl ≃ −0.1 e^-, Pd ≃ −1.1 e^-, Sr ≃1.3 e^- in $SrPdTl_2$ and Tl ≈ −0.65 e^-, Sr ≈ +1.3 e^- for $SrTl_2$. Thus the insertion of Pd metal corresponds to a partial oxidation of Tl metal with charge transfer to Pd. The H_{ii} values and the large overlap population (Figure 3) are in accord. A somewhat greater effect would be expected with Pt.[25]

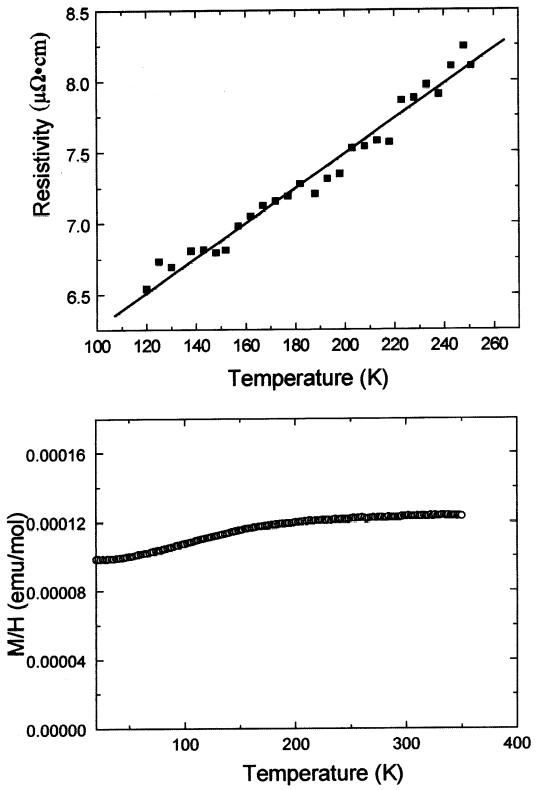

Figure 5. Resistivities ($\mu\Omega$·cm) (top) and molar magnetic susceptibilities (emu mol^{-1}) (bottom) of $SrPdTl_2$ as a function of temperature (K).

Physical Properties. The resistivities of powdered $SrPdTl_2$ increase linearly with temperature, as shown in the top part of Figure 5. The isotropic resistivity is about 9.2 $\mu\Omega$ cm at room temperature, with a mean temperature dependence of 0.34% K^{-1}. This indicates that $SrPdTl_2$ is a fairly normal, "good" metal. The small molar magnetic susceptibilities of $SrPdTl_2$ are shown in the bottom part of Figure 5. The compound is essentially Pauli-paramagnetic with $\chi_m \simeq 1.2 \times 10^{-4}$ emu mol^{-1} above ∼200 K, in agreement with expectations.

Acknowledgment. We are indebted to S. Budko for the magnetic susceptibility data.

Supporting Information Available: Tables of more data collection and refinement parameters and anisotropic displacement values for $SrPdTl_2$. This material is available free of charge via the Internet at http://pubs.acs.org.

IC030089K